Journal of Renewable Materials
DOI:10.32604/jrm.2020.08618
Article

Tech Science Press

Pyrolysis of Rice Husk in a Fluidized Bed Reactor: Evaluate the Characteristics of Fractional Bio-Oil and Particulate Emission of Carbonaceous Aerosol (CA)

Ning Li[1,2], Weiming Yi[1,2], Zhihe Li[1,2,*], Lihong Wang[1,2], Yongjun Li[1,2], Xueyuan Bai[1,2] and Mei Jiang[1,2]

[1]School of Agricultural Engineering and Food Science, Shandong University of Technology, Zibo, 255000, China
[2]Shandong Research Center of Engineering and Technology for Clean Energy, Zibo, 255000, China
*Corresponding Author: Zhihe Li. Email: lizhihe@sdut.edu.cn
Received: 16 September 2019; Accepted: 18 November 2019

Abstract: Bio-oil production via pyrolysis is one of promising technologies for renewable energy production from bio-wastes. However, the complicated bio-oil is still a challenge for high-valued application and during biomass pyrolysis, the emission of non-cleaned aerosol, the potential emission, namely carbonaceous aerosol (CA) increased the difficulty of the commercial promotion. In this study, Rice husk pyrolysis was performed in a semi-continuous fluidized bed reactor coupled with fractional condensers. The effects of pyrolysis and condensation temperature on the properties of bio-oil and emission of CA were investigated systemically. Results indicated that the in-situ separation of vapors was accomplished via condensers of different temperatures (85°C and −10°C). The bio-oil with different physiochemical properties were obtained in the high content of phenols and lower acids of BO1 and high content of acids and better liquidity. The size distribution of CA was found primarily classified as sub-micrometer grade particles, which have a diameter of less than 1.1 μm. In particular, CA existed in three representative forms: bead, granular aggregate, and liquidoid. The results of light absorption of total organic carbon (TOC) and non-volatile organic carbon (NVOC) indicated that the absorption per mass increased in the single temperature with the decrement of wavelength and it improved as the pyrolysis temperature increased at the specified wavelength. The absorption per mass was to maximum value (3.7 m^2/g) at 360 nm wavelength and 600°C. TOC demonstrated a strong light absorption and a wide spectral range dependence (AAE: 5.08-10.05) which enhanced the light absorption in the ultra-violet and low-visible regions.

Keywords: Rice husk; pyrolysis; bio-oil; aerosol; size distribution; light absorption

1 Introduction

Biomass is considered an important substitutive energy product to promoting the sustainable development of society due to its unique features, such as renewability, abundance, carbon neutrality, and low content of heteroatoms including S and N [1,2]. Nevertheless, there are still some challenges to be conquered from waste to energy, that includes its limited energy density, distinct seasonality, complex

chemical composition, and high transportation and storage costs [3-5]. Thermochemical, biochemical and physical conversion technologies have been developed to produce bio-based fuels, materials or chemicals [6].

Fast pyrolysis as one attractive thermochemical technology [7,8] is performed in an oxygen-free atmosphere between 400°C and 600°C, which causes the breakdown of polymers and subsequently reformation of these compounds into bio-oil, char, non-condensable gas (NCG) and persistent aerosol [9-11]. Previous studies have been carried out and mainly focused on the effect of various factors, such as operating parameters (e.g., pretreatment, feedstock category, temperature and catalyst), reactor [12-15] and pyro-oil refining [16]. In addition to these factors, condensing system is equally important to the main section of reactor in pyrolysis process. It is used to recover the vapors into bio-oil that directly determines the yield and quality of bio-oil and efficiency of subsequent upgrading [17]. Single or multi-stage condenser (spray tower, other shell and tube condenser or their combination) can produce one mixed liquid which contained much water and light carboxylic acids accelerating aging and reducing the quality of bio-oil, and even mingle with another cooling media that aggravated compounds separation [17]; Oppositely, fractional condensation system consist of two or more different temperature exchanger tube where different bio-oils can be got in the properties of physical and composition during primary in-situ condensation [17]. And it offered a possibility way to later explore the different application [18,19] compared to the traditionally complicated oil and it have attracted more attention [20,21]. In the process of collecting condensable vapors, a series of condensable tubes with gradient temperature are set for capture organic molecules of different dew point. Generally, when the partial pressure of condensation environment is below 0.24 atm, phenols, sugars and other lignin- or cellulose-derived macromolecules can be commonly condensed at up to 80°C and the acids, water and other micromolecules can be gathered at the low temperature [22]. Pollard et al. [23] developed a fractional bio-oil recovery system to achieve the low water content (7-15 wt.%) and reduced acid content up to 50 wt.%. Specifically, water could be effectively separated from the bio-oil to significantly increase the calorific value of the oil, up to 31 MJ/kg [24]. And it is significant to improve refining efficiency in catalytic process where water-contained decreased the deactivation of catalyst [25]. Yin et al. [26] investigated the characteristics of products in a fluidized bed reactor coupled with similar temperature condensers (23.5-37°C). The first stage bio-oil has exceeded half water content that caused the lower viscosity. The bio-oil in latter condensers has a higher pH and heating value, similar rate of H/C and O/C, which was also observed in Chen et al. [27]. However, the enrichment of specific compounds cannot be achieved by this method. Ma et al. [19] studied the characteristics of multipurpose bio-oil in a three fractional condensation (110°C, 0°C, −196°C). The carrier gas flow rate has minimal effects on the yield of bio-oil. However, the cooled temperature had a distinct effect on the distribution of compounds. When the cooled temperature was set up to 110°C, abundant phenolic compounds are rich. In the 0°C condenser, light molecule composition mainly contained acids, alcohols, ketones, et al. and water content is very high. At the lowest cooling temperature, hydrocarbons and furans are the maximum yield and it contained a fair amount of water. Furthermore, based on the physical and chemical properties, the separation technologies were applied including molecular distillation, solvent extraction, column chromatography, catalytic hydrogenation and cracking [28-30] to the wider application.

However, biomass pyrolysis is not a zero emission technology [31]. Primary aerosol ejected from biomass pyrolysis suffered from collision and aggregation via vapors condensation to form secondary aerosol. It has similar aerodynamic with carrier gas to easily escape from the traditional condensers to impact downstream equipment, e.g., fouling faces and depositing on the pipe [32], and even polluting the environment. In commercial pyrolysis process, aerosol is commonly treated as aggressive substance and a previous method has been proposed that an electrostatic precipitator was employed to capture aerosol of non-condensable gases [23,24,31]. The ESP arranged in the afterbody of collection system can got 13.3 wt.% mass ratio of biomass [24,31]. In addition, toxic gas (NO_x, CO, HCl et al.), carbonaceous

aerosols (all kinds of organic compounds) [33] and minerals may also be emitted when pyrolysis temperature was increased [31]. Teixeira et al. [34] investigated the cellulose doped with calcium pyrolysis by laser diffraction light scattering, inductively coupled plasma spectroscopy. The primary aerosol ejected through the boiling bubble from the liquid intermediate cellulose. The inorganic calcium by bubbling ejection was transported through the generation of primary aerosol. The emitted aerosol (organic and inorganic) accounts for approximately 3% of raw material. And the mass distribution of aerosol mainly focused in the size of 10 nm to 200 nm. Jendoubi et al. [31] focused on the distribution of inorganic species through performing wheat straw and beech wood fast pyrolysis in a fluidized bed reactor coupled with an electrostatic precipitator (ESP) to capture aerosol. Over 60 wt.% inorganic content in the whole bio-oil originates from aerosol. The issues are responsible for the observation that aerosol transports the inorganics into bio-oil or extremely fine particles (bio-char) escaped with carrier gas into bio-oil. Iisa et al. [32] studied the concentration and size distribution of aerosol in two pyrolysis systems. The mass-based aerosol diameter mode was mainly 1 μm, but the number-based diameter was < 0.1 μm. And the centrifugal mist separator had high efficiency for removing the particulate of > 0.4 μm diameter. Wiinikka et al. [35] investigated the inorganic species transportation in the cyclone pyrolysis reactor. For the easy volatilized elements such as sulfur and potassium have a large amount of 1-10 wt.% in the bio-oil, especially in the aerosol fraction. Hence, if not handled properly, the aerosol would not only bring about operational problem of downstream process, but also reduce the atmospheric visibility and even have a threat to human health. One aspect that is the emission of fine particles, especially PM_{10} and $PM_{2.5}$, which can enter into the lungs through respiration and then break up the balance of gas-blood interchange [36]. Another aspect it cannot be overlooked is that aerosol particles can absorb and scatter solar radiation [37], especially for the carbonaceous aerosol (CA) which is composed of mostly organic carbon (OC) and small amounts of black carbon (BC) [38]. It is significant in the light absorption to affect the photochemistry of atmosphere and even change the visibility. Although investigations concerned with the light absorption of primary CA have primarily focused on the resulting type of BC emission in the atmospheric environment [39-41], organic aerosol (OA) also termed “brown carbon (BrC)” as the major fraction of atmospheric aerosol was attracted to a growing concern in recent years and evidences showed OA had a strong effect on the radiative forcing at near-UV and shorter visible wavelengths [36,42]. Due to the promise that pyrolysis holds as an alternative energy-producing technology (bio-oil and char), the environmental concerns associated with the emission and prevention of aerosols must be addressed in order to further commercial promotion. However, limited researches have been proceeded to specifically investigate the physical and chemical characteristics of emitted aerosol during pyrolysis process [43].

The objective purpose of this present work is to: 1) Characterize fractional condensational bio-oil produced from pyrolysis, which provides information for value-added compound production; 2) understand the properties of CA (size distribution and morphology) and the optical absorption properties of OA to serve as the basis for estimating the radiative effect of OC and mitigating health risks associated with this type of CA emission. All of quantification and property analysis were carried out in a self-developed and semi-continuous fluidized bed pyrolysis reaction system.

2 Materials and Methods

2.1 Materials

Rice husk was gathered in season from the surrounding farmland of Mashang Town, Shandong Province, China. After dried naturally, rice husk was ground and sieved to a particle size ranging from 0.25 mm to 0.4 mm and stored in a sealable bag. The proximate analysis, ultimate analysis and higher heating value were tested and presented in Tab. 1.

Table 1: Physical and chemical properties of rice husk

Proximate analysis [ad] *(wt.%)*		*Ultimate analysis*[ad] *(wt.%)*	
Moisture	8.61 ± 0.15	C	40.7 ± 0.67
Ash	15.86 ± 0.21	H	5.24 ± 0.23
Volatile	62.68 ± 0.67	N	0.47 ± 0.04
Fixed carbon[b]	12.85 ± 0.6	O[b]	53.59 ± 0.79
HHV(MJ/kg)	15.83		

[ad]Air dry basis
[b]By difference

2.2 Fast Pyrolysis Unit and Aerosol Sampling System

Fast pyrolysis experiments were conducted in a bubbling fluidized bed reactor, for the capacity of 3 $kg{\cdot}h^{-1}$. In order to ensure the complete pyrolysis reaction, feeder rate was perfected controlled at 16.5 $g{\cdot}min^{-1}$ through the synergistic action of rotary scraper and screw (refer to the attachment for detailed information concerning the relationship of speed and feeding rate and the specified structure has been described in [44] and the supplementary information Fig. A1). The cylindrical reactor was made of stainless steel (316 s) with an internal diameter of 50 mm and a height of 800 mm. Inert silica sand, which was 70 mm in height, was used as fluidizing agent distributing on the plate. Nitrogen (purity of 99.99%) entered into reactor as the inert fluidization gas at a flow rate of 2.2 $m^3{\cdot}h^{-1}$. Two-stage cyclones were connected to remove particulate matter from the output gas stream and heated to 360°C to avoid vapors condensation prior to reaching the condenser. A ring heater and a plate heater were respectively used for the reactor and cyclones. The heater was independently monitored and regulated using a proportional integral differential (PID) controller which provided a stable temperature zone. Trial experiments were conducted to discern the number and arrangement of condensers required which was determined based on the optical collection efficiency. Four groups of two-stage glass condensers were set up in series and subsequently injected with two temperature cooling media at 85°C and −10°C, respectively. The first two-stage coolers were classified as the first condensable unit, and the other was the second condensable unit which contained an ahead Allihn condenser and a back Spiral condenser. As shown in Fig. 1, CA was simultaneously collected by two types of impactor (Aerosol sampler 1 and Aerosol sampler 2) for further analysis regarding the mass size distribution, morphology and light absorption properties. Aerosol sampler 1 was a filter for the CA complete collection; Aerosol sampler 2, referred to as the Andersen impact sampler, demonstrated excellent performance for size segregation of aerosol particulates by dividing aerosol particles into different size ranges [33]. According to Fu et al. [45], the low-volume sampler was found to have a better separation efficiency and higher accuracy depending on the design specification and number of stages. Hence, a homemade, low-volume sampler (28.3 $L{\cdot}min^{-1}$) was equipped, which was equipped with seven stages of inertial impactors and a back-up filter. The quartz filter (Munktell 360, Munktell Filter AB Inc.) was used to collect aerosol particles at different stages of the impactor and the complete aerosol. The filter was baked in a muffle furnace at 550°C at least 4 h prior to experiments to reduce blank carbon levels and was stored individually in Petri dishes lined with aluminum foil.

2.3 Products Analyses

2.3.1 Product Mass Balance

Bio-char as the by-product produced after biomass pyrolysis mainly distributed in the bed material, the surface of the cyclones' wall, char collector and bio-oil. Hence, nitrogen gas was allowed to flow for a few

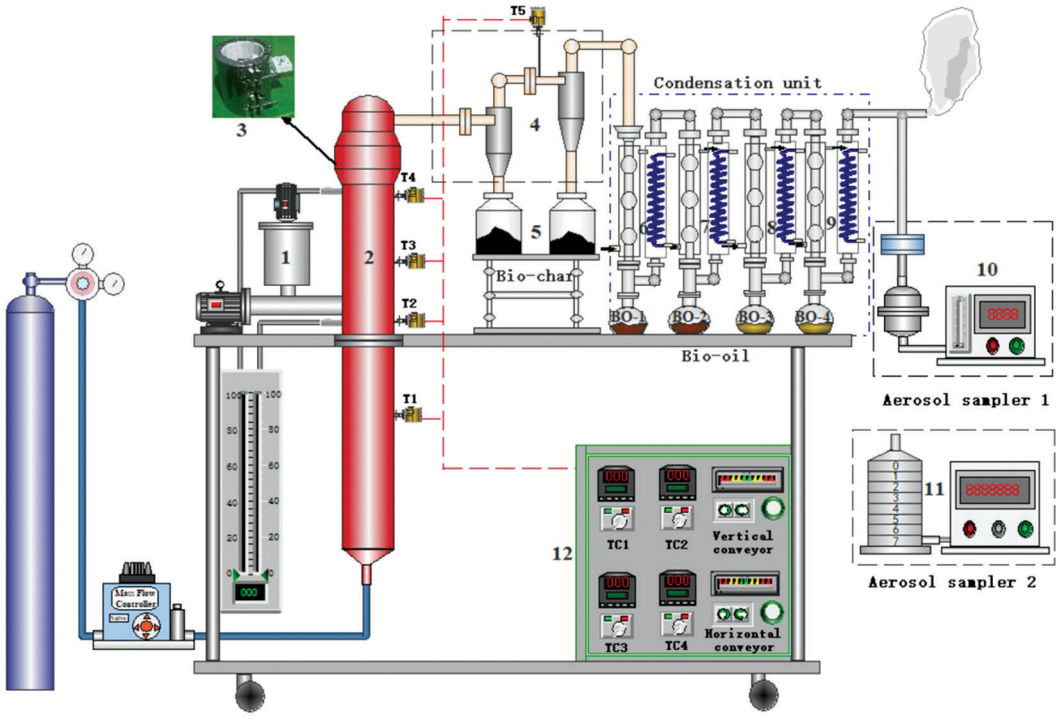

Figure 1: Schematic of the bubbling bed reactor pyrolysis reactor coupled with fractional condensation units

minutes to trap the reactor char. And the content of char in the bio-oil was assumed to be negligible based on the high separation efficiency of the cyclones and strict screening of raw material in prior period. The char content was calculated by weighing the mass of the cyclones and two-stage char collectors before and after each experiment. The liquid fraction was defined as the first fractional bio-oil (BO1) and second fractional bio-oil (BO2), and was weighed prior to conducting analysis. When the experiment was stable, a filter was set after the outlet and completely pumped for 2 minutes. The calculation of the quality of CA sample and the feeding rate described above represents the yield of CA. The yield of NCG (non-condensable gas) was calculated by weight difference.

2.3.2 Physicochemical Properties of Fractional Bio-Oils

Water content: The water content of fractional bio-oil samples was measured with a volumetric Karl Fischer Titrino (Metrohm Switzerland, Model 870 plus).

Kinematic Viscosity and pH: The kinematic viscosity of the samples was tested by a automatic kinematic viscosity tester (Kulun Zibo, Model YDH100). The pH of the samples was determined using a pH meter (Leici Shanghai, Model PHS-3G).

The components of bio-oil: Because of the complicated compounds of bio-oil, the accurately quantitative analysis of bio-oil was difficult to be achieved. Whereas, the relative peak area % of the GC-MS chromatogram was considered to be a good approximation, it presents the relative amount of the various chemical compounds in the bio-oil [46,47]. Chemical components were detected via a Gas Chromatography-Mass Spectrometer (GC/MS) (Agilent, Model 5973-6890N) with a DB-1701 capillary column. The temperature of the injector and Aux was set at 280°C and 250°C, respectively. The oven temperature of the GC was ramped from 40°C to 240°C with a heating rate of 5°C·min^{-1}, and then held for 5 min. High purity Helium (99.999%) was used as a carrier-gas with a constant flow rate of

1 mL·min^{-1}. The injection volume was 0.2 μL, and the split ratio was 60:1. The MS analysis was operated in EI mode with an ionization energy of 70eV and a scanning range of (m·z^{-1}) 12~550 amu. The detailed information concerning the identification of chromatographic peaks was determined based on the NIST-MS 2.0 library.

2.3.3 Particle Distribution and Physical Structure

The sampling period was 3 min for aerosol sampler 1 and aerosol sampler 2. At the end of the sampling, the filters were returned to the dishes immediately and stored in a freezer (−20°C) until further analysis was conducted. The sample in sampler 1 was weighed before and after each experiment concluded. Then, the sample was conducted to the visual observations of the micro-structure of the sample using a scanning electron microscope (SEM Quanta 250FEG) for the different sizes of aerosol.

2.3.4 Light Absorption of OC

Due to the existence of second volatile organic compounds (SVOC) in the total OC matter easily causing the secondary emission in the ambient condition, SVOC can lead to the secondary pollution. Hence, SVOC would be removed at 170°C under an inert, nitrogen atmosphere to determine the effect on the light absorption [38]. The extraction and characterization of spectral light absorption of OC samples before and after drying were conducted. The specific methods utilized for this analysis were implemented according to the methodology reported by Li et al. [37] and Chen et al. [38]. A quarter of quartz filter before and after heating at 170°C with 3.5 ml methanol were sealed and sonicated for 5 h at room temperature (25°C) to ensure complete extraction. All the extracts were filtered with a 0.2 mm pore size syringe filter to remove impurities. Then, 40 μl of the extract was pipetted onto a blank 4 cm^2 quartz filter, and the sample was dried for 1 h in a fume hood. The OC concentration in the extracts was tested by a thermal-optical OC/EC (organic carbon/elemental carbon) analyzer (Sunset Laboratory, Tigard, Model RT4). Finally, the light absorption of TOC (total organic carbon) and NVOC (non-volatile organic carbon) samples were measured using a UV-vis spectrophotometer (Shimadzu, UV-3600Plus) with a wavelength spectra ranging from 200 nm to 800 nm.

The main values determining the particle's optical properties of OC in this article include the light absorption per mass of organic carbon aerosol (α/ρ), imaginary refractive index (k_{OA}) and absorption Ångström exponent (AAE). The specific derivations of these values were determined based on the methodology present in a previous study [38].

3 Results and Discussion

3.1 Pyrolysis Products Distribution

The yield and appearance of BO1, BO2, char and aerosol at different pyrolysis temperatures are reported in Fig. 2. BO1 was a black-brown color with a pungent smell that contained a small amount of fine char powder. BO2 was a russet, water-soluble liquid. The char was a black, fine, solid particle. The mixture of aerosol and NCG presents a pale blue or white smoke after the vapor condensed.

The yield of NCG increased as the temperature increased, reaching a maximum of 26.8 wt.% at 600°C. The similar trend of gas yield was confirmed by Cai et al. [48]. Yet, the increase in aerosol yield raise between 400°C and 500°C, and then it decreases with temperature increasing. The maximum of aerosol content is 11.3 wt.% at 500°C. It may be responsible for the phenomenon that the cracking reactions (depolymerization and fragmentation decarbonylation and decarboxylation reactions) become more intensified from 400°C to 500°C. More vapors containing the aerosol emitted, whereas, when pyrolysis temperature exceeds 500°C, secondary reaction, rearrangement in the polycyclic structure and the conversion of short substitutes are the dominant behavior that contributed to more gas content [49]. In comparison, the char yield continually decreased, reaching a minimum value of 30.3 ± 0.4 wt.% at 600°C. Ma et al. [19] discovered a similar char yield trend in a fixed bed pyrolysis reactor. However, the

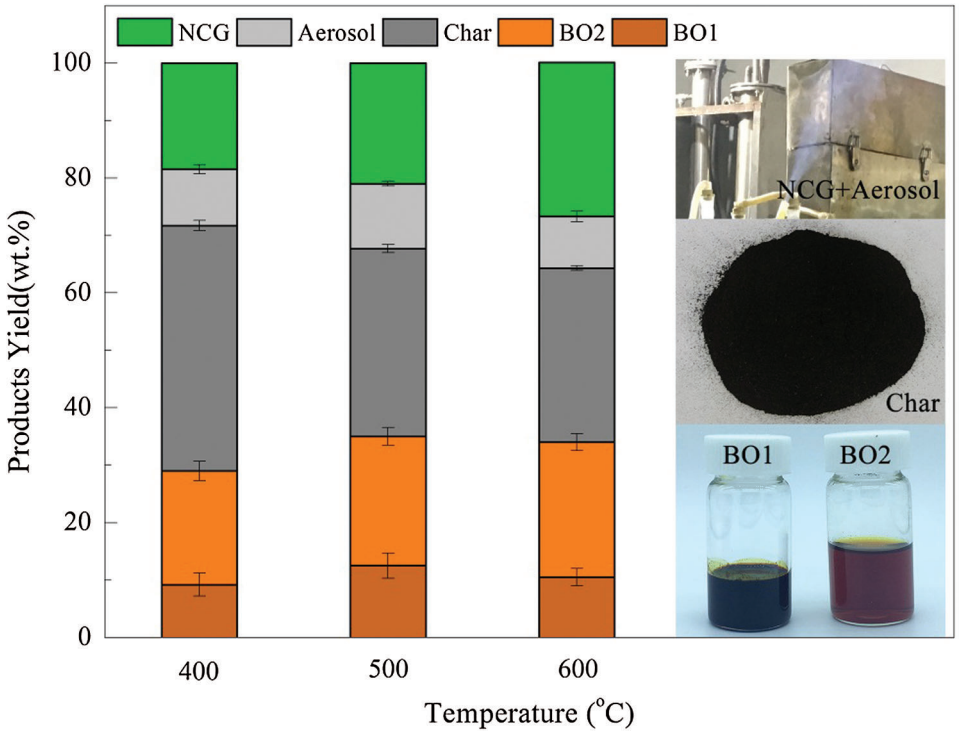

Figure 2: Yields of bio-oil, char, gas and carbonaceous aerosol at different temperatures

changing rate of char yield is relatively small due to rearrangement reaction with the inert biomass and secondary reaction between vapors and char when the material was static. For either BO1 or BO2, the yield increased before 500°C and then showed a negative tendency. At 500°C, the highest yield of total bio-oil was 35 ± 1.5 wt.% was obtained. The BO1 yield showed a similar trend as that of the total bio-oil. A maximum yield of 12.5 wt.% was obtained at 500°C. Gooty et al. [24] studied the fractional condensation of vapors from birch bark in a series of condensation temperatures to get the maximum yield of oil fraction and water fraction at 550°C. The yield of BO2 increased with increasing temperature, and it achieved the highest yield of 23.5 ± 1.5 wt.% at 600°C. At higher temperature, extensive decarbonylation and fragmention caused much small molecule organic compounds which were easily formed in the condition of lower cooling temperature and larger contact area.

3.2 The Physicochemical Properties and Composition of Bio-Oil

The water content, pH and viscosity of BO1 and BO2 at different pyrolysis temperatures are summarized in Tab. 2. The water content of BO1 was one order of magnitude less than that of BO2. And it in BO1 and BO2 increased as the pyrolysis temperature increased, and both trials reached water content values of up to 5.7% and 68.5% respectively at 600°C. Gooty et al. [24] showed the alike trend, but the oil fraction had less amount of water content. The saturation pressure of water was positively correlated with the saturation temperature [23]. The lower temperature of the last condenser led to the accumulation of moisture. The water in BO1 was formed through the precipitation of moisture above the dew point and then by adhering to the wall of the condenser and wide-length contact area. The pH of BO1 ranged from 3.56 to 3.74. In comparison, the pH of BO2 was lower due to the concentration of myriad acid compounds. Either in BO1 and BO2, the pH decreased when temperature increased due to the increase of acids production. Due to the presence of char, macromolecular polymers and lignin-derived compounds, the

Table 2: The properties of bio-oils collected in the condensers of 85°C and −20°C at different pyrolysis temperatures

Temperature (°C)	Water content (wt.%)		pH		Viscosity (mPa·s)	
	BO1	BO2	BO1	BO2	BO1	BO2
400	2.9	56.88	3.74	2.41	876.4	4.2
500	4.8	64.8	3.68	2.24	868.5	2.8
600	5.7	68.5	3.56	2.16	852	2.2

viscosity of BO1 decreased from 876.4 to 852 mPa·s. BO2 had a better liquidity because of its lower viscosity of 2.2 mPa·s at 600°C. The water content was directly related to the pH and viscosity of bio-oil and appropriate water content is beneficial to after treatment and application.

The compounds present within BO1 and BO2 were detected via GC-MS. The primary components of the bio-oil consisted of acids, alcohols, aldehydes, ketones, furans, phenols, esters and sugars. The chemical composition analysis of the bio-oils is elucidated in Tab. 3. In Figs. 3a and 3b, it is illustrated that the content of chemical compounds detected in BO1 and BO2, respectively. BO1 was mainly comprised of phenols and sugars. Conversely, BO2 as water fraction consisted of acids, ketones, furans and aldehydes. The enhanced presence of compounds at different cooling temperatures was related to the dew point of different compounds. As the temperature rose, the relative content of phenols significantly increased in BO1 which was caused by the conversion of aromatic rings and charring processes (380-800°C) [49]. Phenols in BO2 remained basically constant at 3%. Zhang et al. [50] also found an increased presence of aromatic compounds in bio-oil from pyrolysis of sludge when the temperature increased from 450°C to 750°C. The acids present in the bio-oil primarily consisted of acetic acid, propanoic acid, and 2-propenoic acid. The concentration of these acids increased as the temperature increased. It is responsible that hemicellulose and lignin occurred to fragmentation at the stage (150-370°C) based on the constitutional unit [51]. The highest content of acids (22.2 ± 1.75%) in the BO2 sample was achieved at 600°C. Ma et al. [19] obtained discovered a similar trend for the accumulation of acids at different temperatures in the second condenser. As for the sugars, 1,6-Anhydro-á-D-glucopyranose was mainly found in BO1, which is a typical chemical compound derived from glucose. The content of this compound continuously decreased from 6.8 ± 0.6% to 3.31 ± 0.75% with temperature increasing in BO1. The content of furans in both oil fractions remained relatively stable around 5%, and esters showed a similar tendency. Lv et al. [52] studied the pyrolysis of corn stalk at different temperatures. It was found that the content of phenols was the most abundant among all the other chemical constituents. The contents of alcohols, aldehydes and ketones increased first as the temperature increased and then decreased thereafter, whereas the content of acids and furans decreased first as the temperature increased and then increased in the range of 300-900°C thereafter. BO1 has less water contents contributing to high value that is favorable for the combustion point. Simultaneously, high content of phenols can be extracted to apply to synthesizing phenol-formaldehyde resins [20]. BO2 is rich in much acids and ketones and little phenols that can be produced into insecticide through further separation [53].

3.3 Mass Size Distribution and SEM Analysis

Aerosol mass concentration distribution at different stages and different temperatures was measured by an impactor for triplicate times and was shown in Fig. 4. It was observed that the mass distributions at different pyrolysis temperatures showed a unimodal mode with the peaks ranging from 0.43 to 0.65 μm and the mass concentration increased as the temperature increased. The maximum value was 29.07 ± 1.2 $mg{\cdot}L^{-1}$ at 600°C.

Table 3: Chemical compounds in BO1 and BO2 analyzed by GC/MS

No.	Compound	Molecular Formula
1	***Acids***	
	Acetic acid	$C_2H_4O_2$
	Propanoic acid	$C_3H_6O_2$
	2-Propenoic acid	$C_3H_4O_2$
	Butanoic acid, 4-hydroxy-	$C_4H_8O_3$
2	***Alcohols***	
	Methyl Alcohol	CH_4O
	2-Propen-1-ol	C_3H_6O
	Cycbpropylcarbino	C_4H_8O
	2-Cyclopenten-1-one, 2-hydroxy-	$C_5H_6O_2$
	Cyclopentanol	$C_5H_{10}O$
	Dianhydromannitol	$C_6H_{10}O_4$
	Cyclohexen-1-ol	$C_6H_{10}O$
3	***Aldehydes***	
	Formaldehyde	CH_2O
	Acetaldehyde, hydroxy-	$C_2H_4O_2$
	Propanal	C_3H_6O
	Butanedial	$C_4H_6O_2$
	Benzaldehyde, 3-hudroxy-4-methoxy-	$C_8H_8O_3$
	4-Hydroxy-2-methoxycinnam aldehyde	$C_{10}H_{10}O_3$
4	***Ketones***	
	2-Propanone, 1-hydroxy-	$C_3H_6O_2$
	2,3-Butanedione	$C_4H_6O_2$
	2-Butanone, 3-hydroxy-	$C_4H_8O_2$
	1-Hydroxy-2-butanone	$C_4H_8O_2$
	2-Propanone, 1-(acetyloxy)-	$C_5H_8O_3$
	3-Pentanone	$C_5H_{10}O$
	2-Cyclopenten-1-one, 2-methyl-	C_6H_8O
	2-Cyclopenten-1-one, 3-methyl-	C_6H_8O
	2-Cyclopenten-1-one, 2-hydroxy-3-methyl-	$C_6H_8O_2$
	2-Butanone, 1-(acetyloxy)-	$C_6H_{10}O_3$
	Ethanone, 1-(2-hydroxy-5-methylphenyl)-	$C_9H_{10}O_2$
5	***Furans***	
	2(5H)-Furanone	$C_4H_4O_2$
	2,3-Dihydrofuran	C_4H_6O

(Continued)

Table 3 (continued).

No.	Compound	Molecular Formula
	Furfural	$C_5H_4O_2$
	2-Furanmethanol	$C_5H_6O_2$
	2,4(3H,5H)-Furandione, 3-methyl-	$C_5H_6O_3$
	2-Furanol, tetrahydro-2-methyl-	$C_5H_{10}O_2$
	2-Furancarboxaldehyde, 5-methyl-	$C_6H_6O_2$
	2-Furancarboxaldehyde, 5-(hydroxymethyl)-	$C_6H_6O_3$
	Benzofuran, 2,3-dihydro-	C_8H_8O
6	***Phenols***	
	Phenol	C_6H_6O
	Hydroquinone	$C_6H_6O_2$
	1,2-Benzenediol	$C_6H_6O_2$
	Phenol, 2-methoxy-	$C_7H_8O_2$
	Phenol, 2-methyl-	C_7H_8O
	Phenol, 4-methyl-	C_7H_8O
	Phenol, 2,4-dimethyl-	$C_8H_{10}O$
	Phenol, 4-ethyl-	$C_8H_{10}O$
	Phenol, 2-methoxy-4-methyl-	$C_8H_{10}O_2$
	Phenol, 2,6-dimethoxy-	$C_8H_{10}O_3$
	1,4-Benzenedicarboxaldehyde, 2-methyl-	$C_9H_8O_2$
	2-Propenoic acid, 3-(2-hydroxyphenyl)-, (E)-	$C_9H_8O_3$
	2-Methoxy-4-vinylphenol	$C_9H_{10}O_2$
	Phenol,2-methoxy-6-(2-propenyl)-	$C_{10}H_{12}O_2$
	Phenol, 4-ethyl-2-methoxy-	$C_9H_{12}O_2$
	Phenol, 4-(3-hydroxy-1-propenyl)-2-methoxy-	$C_{10}H_{12}O_3$
	Phenol, 2-methoxy-4-(1-propenyl)-	$C_{10}H_{12}O_2$
7	***Esters***	
	Acetic acid, methyl ester	$C_3H_6O_2$
	Butyrolactone	$C_4H_6O_2$
	2-Propenoic acid, ethenyl ester	$C_5H_6O_2$
	Propanoic acid, 2-oxo-, methyl ester	$C_4H_6O_3$
8	***Sugar***	
	1,6-Anhydro-á-D-glucopyranose	$C_6H_{10}O_5$

Most aerosol particulates are distributed at a range of less than 2.1 μm. These fine particulates are extremely permeable and thereby have the ability to enter the lung and even the blood through respiration [54]. As the pyrolysis temperature increased from 400 to 500°C, the mass concentration of aerosol particles with a size

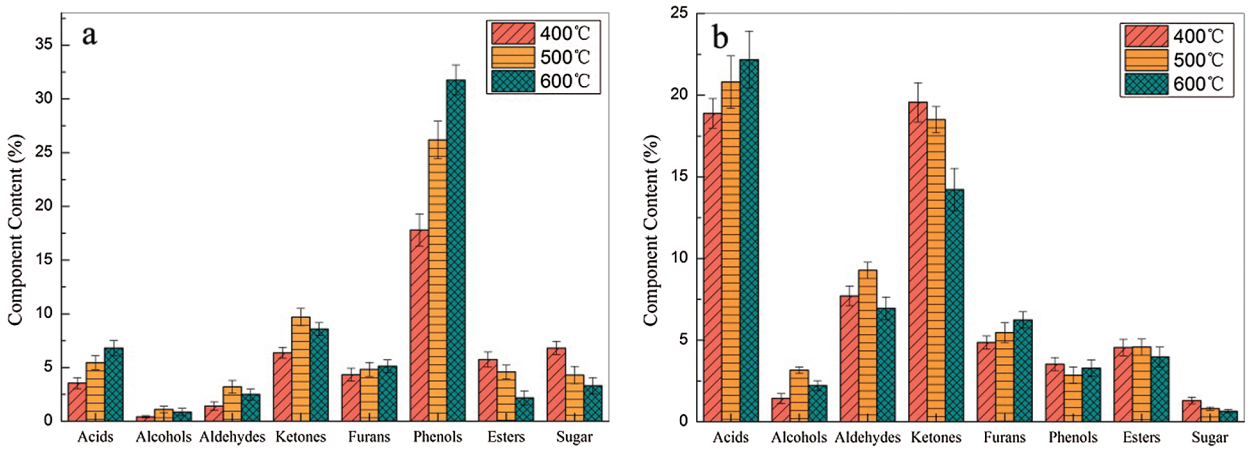

Figure 3: The major chemical components present within BO1(a) and BO2(b)

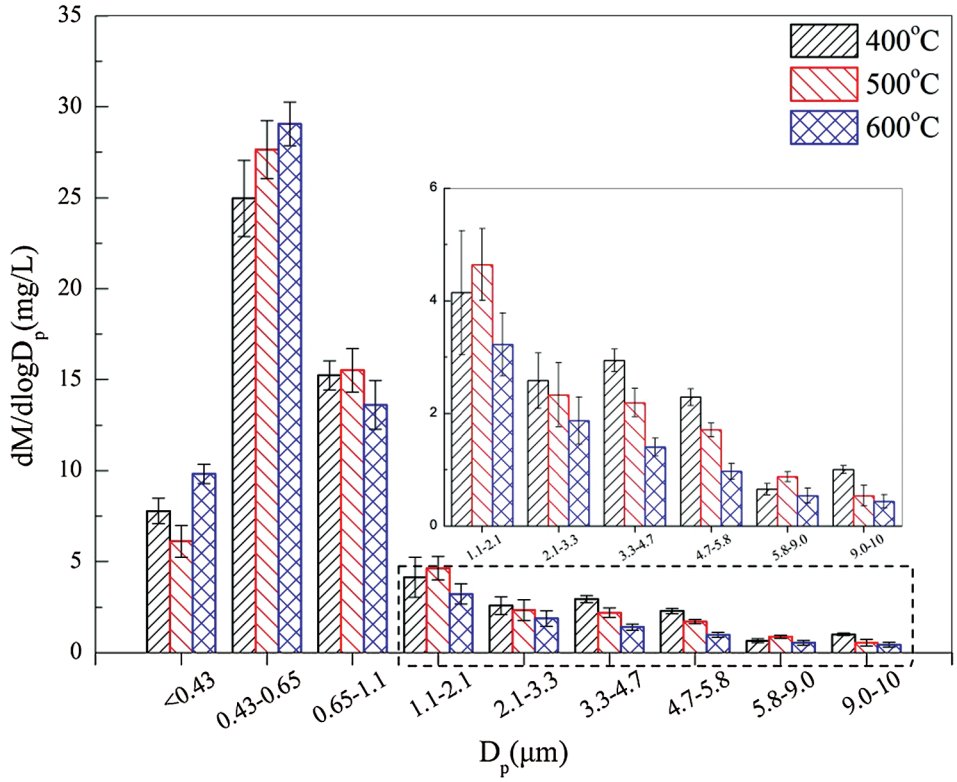

Figure 4: Particulate mass size distribution at different temperatures

larger than 2.1 μm significantly decreased up to 86%. In contrast, sub-micron grade particles (aerosol size less than 1 μm) increased slightly. High temperatures led to the production of a greater concentration of aerosol emission; especially for the sub-micron particulates has a larger cardinal number. Fig. 5 presents the appearance of 0 (> 9 μm), 3 (3.3-4.7 μm), 7 (0.45-0.65 μm), 8 (< 0.43 μm) and morphology of aerosol particulates collected by the filter at 500°C. As it can be seen, each filter can be obviously separated into two zones. First, the brown spot was formed due to the impact of aerosol particles in the corresponding size

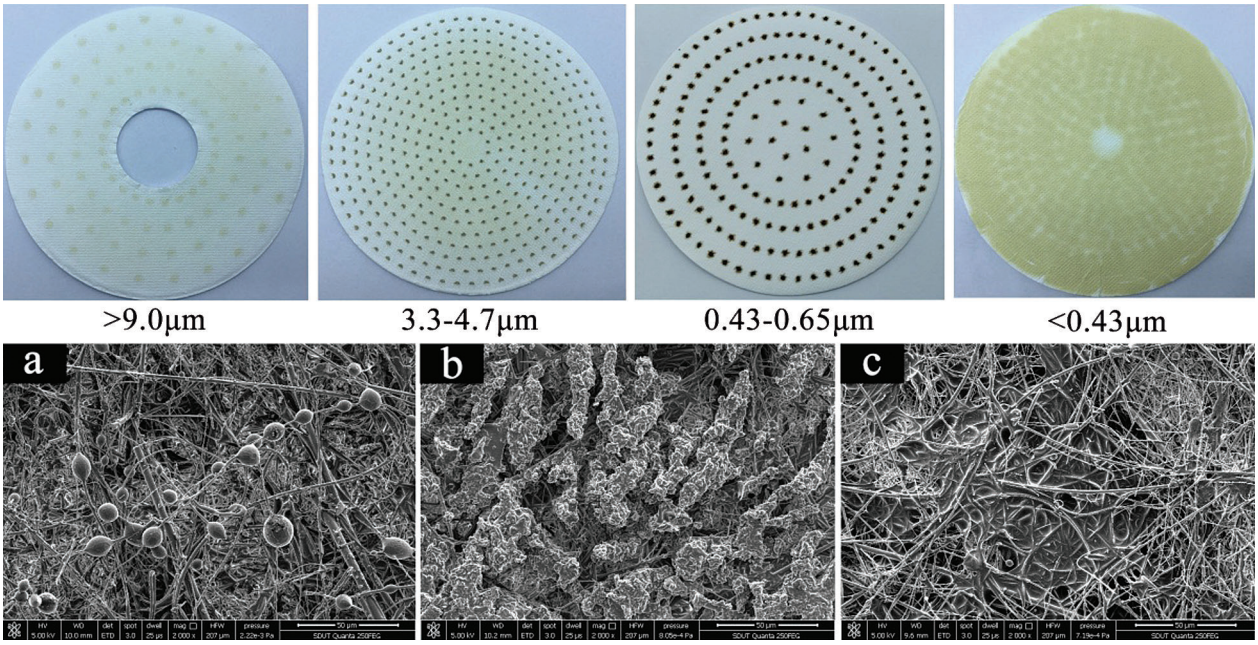

Figure 5: The aerosols with nine impactor stages and SEM analysis

range. Second, the light-colored area indicated that aerosol particles were intercepted by the fibers of the filter. The color of the spot changed from yellow to black-brown as the size of the filter decreased from 10 μm to 0.43 μm and then changed to a light yellow color at a filter size range of less than 0.43 μm. A clearly visible spot was observed when the size of aerosol particulates was greater than 1.1 μm. However, the spot was blurry at the range of 1.1-0.65 μm. SEM analysis illustrated that the aerosol structure can be classified into three types, as shown in Fig. 5. The aerosol particle had different physical structures at the different size ranges. The aerosol existed in the bead (Fig. 5a) form and was interlaced within the fibers, which was generated through the single aerosol droplet adhered to the fiber. Granular aggregates were also observed in Fig. 5b that indicated the aerosol or fragment collided with each other in the process of movement and that easily caused deposition in the pipeline. Fig. 5c presents the liquid area which was caused by the aggregation of the imperceptible droplets, which has strong stickiness and cannot be removed effortlessly.

3.4 Optical Properties of OC

In this paper, the light absorption of OC of aerosol at different pyrolysis temperatures of 400°C, 500°C and 600°C was investigated. SVOC had a significant ratio of the TOC mass. The SVOC contributed 59.3%, 56.5% and 51.8%, respectively, to the TOC value based on the detection of TOC and NVOC (supplementary information Tab. A1). When pyrolysis temperature increased, the cracking and recombination of vapor were serious, which are responsible for the reduction of produced SVOC. Fig. 6 shows the absorption per mass of TOC and NOVOC ($^{\alpha}/_{\rho}$). Generally, $^{\alpha}/_{\rho}$ of TOC and NVOC decreased as λ increased. In the range of ultraviolet and shorter visible wavelength, the $^{\alpha}/_{\rho}$ showed a strong light absorption effect. For the TOC, the $^{\alpha}/_{\rho}$ enhanced by 12.2% when the temperature rose from 400°C to 500°C, and it increased approximately 13.3% with an increase to 600°C. When λ was at 360 nm, $^{\alpha}/_{\rho}$ of OC was 2.94, 3.30 and 3.74, respectively from 400°C to 500°C. The absorption per mass of NVOC showed a similar change with wavelength, but the value is relatively lower than TOC owing to the removal of SVOC. The results were similar to that results presented by Li et al. [37] and Chen et al. [38], which detected the $^{\alpha}/_{\rho}$ value of wood and corn stalk at 210°C, 270°C and 360°C, but the difference between the values was relatively

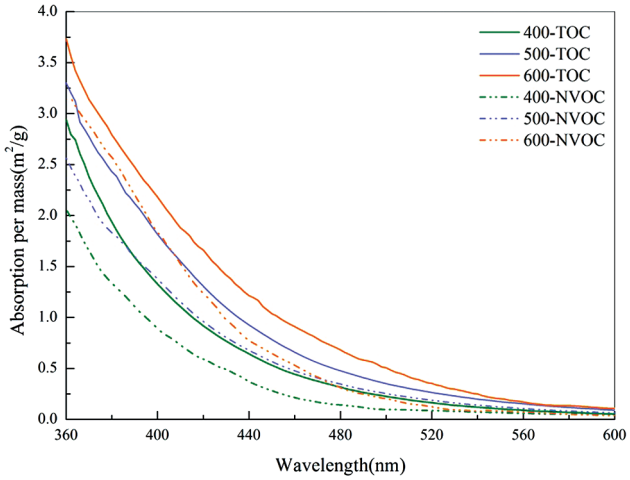

Figure 6: Absorption per mass of TOC and NVOC (α/ρ) at three pyrolysis temperatures

large due to the different material structure and pyrolysis temperature. At a higher pyrolysis temperature range, different cracking modes of organic macromolecules occurred and the condensation collected most condensable volatiles that maybe responsible for the above results of light absorption. Before 400°C, the dehydration of three constituents were complete; between 400°C and 500°C, conversion of the short substituents of the aromatic rings and rearrangement in polycyclic structure occurred, and the small molecular SVOC may crack to gas or combine to form larger molecular. At a higher temperature (600°C), the excess arrangement of aromatic rings present within lignin was the dominant reaction pathway [55,56]. When aerosol included more aromatic polymers [57], the light absorption showed stronger [36]. Hence, the highest absorption per mass of 3.74 was observed. α/ρ of NVOC was significantly lower than that of the TOC and SVOC, and it is an important indicative factor that determines the property of aerosol light absorption.

Values of k_{OA} at different pyrolysis temperatures were reported in Fig. 7, which is an internal property. For TOC and NVOC, k_{OA} declined when the wavelength became longer. In particular, the k_{OA} for TOC varied from 0.1 to 0.13 at a wavelength of 360 nm, and for NVOC it varied from 0.07 to 0.11 at the same wavelength. Kirchstetter et al. [57] investigated the k_{OA} of wood burning and biomass smoke

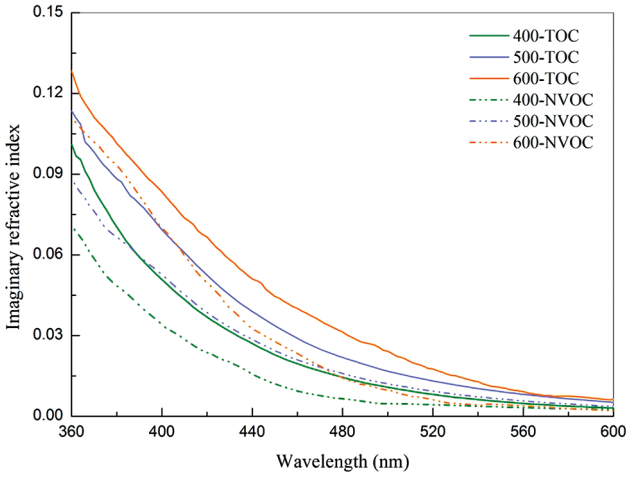

Figure 7: Imaginary part of the refractive index (k_{OA}) at three pyrolysis temperatures

samples extracted by acetone which were collected on quartz fiber filters. In the detection wavelength range, the k_{OA} showed a larger range, and its maximum value at 360 nm was more than one time higher than the value in this study. Chakrabarty et al. [58] conducted fuel combustion to investigate the optical properties of smoke particle emissions, in which a much lower value was reported. In addition, it was also found that a wavelength-independent component, k_{BC}, occurred in the very small BC volume fraction.

As shown in Fig. 9, AAE for OC obtained from 400 to 600°C ranged from 5.08 to 10.06 in the whole spectral region. OC showed strong spectral dependence in organic aerosol except for black carbon [57]. Values of AAE for TOC changed significantly from 5.08-8.02, and this value sharply decreased at 500°C. The difference in the NVOC was caused by the SVOC. At the same level of temperature, AAE for NVOC was higher than that for TOC, which indicated that it contained weaker light absorption particles than TOC. The AAE increased along with the absorption per mass at 600°C. Those values were similar to the values obtained by Chen et al. [37]. However, this paper demonstrated higher values and a wider range than the values reported by Chakrabarty et al. [58] for fuel combustion (2.7-6.8) and Li et al. [37] for corn stalk pyrolysis (7-7.7). The different heat treatment conditions and different post-processes caused different aerosols to be emitted.

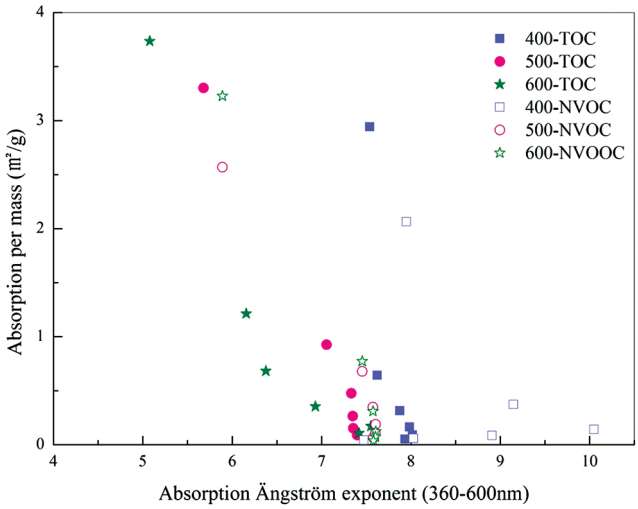

Figure 8: Absorption Ångstrom exponent (AAE) (from 380 nm to 600 nm) *vs.* α/ρ at 400 nm

4 Conclusions

Rice husk was pyrolyzed in a fluidized bed reactor coupled with a series of two temperature controlled indirect condensers. The physical and chemical properties of bio-oils were investigated utilizing fractional distillation and the emitted aerosol was analyzed according to its mass size distribution, morphology and features of light absorption of OC. As the temperature increased, the highest yield of BO1 was obtained at 500°C, whereas the highest BO2 yield was 23.5 wt.% which was obtained at 600°C. From 400°C to 600°C, the ratio of aerosol changed in the range of 9 and 11.3 wt.%. BO1 had a higher content of phenols and sugars in comparison with BO2. The latter contained more water, aldehydes, ketones and acids, thereby having a better liquidity. The maximum value of aerosol concentration was 29.07 ± 1.2 $mg{\cdot}L^{-1}$ at the size of 0.43-0.65 at 600°C. CA primarily consisted of sub-micrometer particulates that existed in three representative forms, including bead, granular aggregate and liquidoid. The absorption per mass of TOC and NVOC decreased as the wavelength increased and their maximum value of α/ρ was 3.74 and 3.23, respectively, at a temperature of 600°C. The absorption of OC showed a strong and wide

spectral dependence (AAE: 5.08-10.06). The OC had an important effect on the optical absorption. All of the aforementioned conclusions lay the groundwork for providing a fundamental understanding of aerosol features for proposing the solution for clean utilization of pyrolysis technology.

Acknowledgement: The authors gratefully thank the support for this research from the Project supported by Shandong Provincial Natural Science Foundation of China [ZR2017MEE004]; National Natural Science Foundation of China [51536009 and 51276103]; Distinguished Expert of Taishan Scholars (Shandong Province) and Higher Education Superior Discipline Team Training Program of Shandong Province, China National Natural Science Fund [51606113]; Key Research and Development Program of Shandong Province [2017GGX40108].

Conflicts of Interest: The authors declare that they have no conflicts of interest to report regarding the present study.

References

1. Fuentes-Cano, D., Salinero, J., Haro, P., Nilsson, S., Gómez-Barea, A. (2018). The influence of volatiles to carrier gas ratio on gas and tar yields during fluidized bed pyrolysis tests. *Fuel, 226,* 81–86. DOI 10.1016/j.fuel.2018.03.171.
2. Isahak, W. W. M., Hisham, M., Yarmo, A., Taufiq-Yap, Y. H. (2012). A review on bio-oil production from biomass by using pyrolysis method. *Renewable and Sustainable Energy Reviews, 16(8),* 5910–5923. DOI 10.1016/j.rser.2012.05.039.
3. Abdullah, H., Wu, H. (2009). Biochar as a Fuel: 1. Properties and grindability of biochars produced from the pyrolysis of mallee wood under slow-heating conditions. *Energy & Fuels, 23(8),* 4174–4181. DOI 10.1021/ef900494t.
4. Delivand, M. K., Barz, M., Gheewala, S. H. (2011). Logistics cost analysis of rice straw for biomass power generation in Thailand. *Energy, 36(3),* 1435–1441. DOI 10.1016/j.energy.2011.01.026.
5. Hu, Z., Wang, X., Adeosun, A., Ruan, R., Tan, H. (2018). Aggravated fine particulate matter emissions from heating-upgraded biomass and biochar combustion: the effect of pretreatment temperature. *Fuel Processing Technology, 171,* 1–9. DOI 10.1016/j.fuproc.2017.11.002.
6. Vassilev, S. V., Baxter, D., Andersen, L. K., Vassileva, C. G., Morgan, T. J. (2012). An overview of the organic and inorganic phase composition of biomass. *Fuel, 94,* 1–33. DOI 10.1016/j.fuel.2011.09.030.
7. Shen, D., Jin, W., Hu, J., Xiao, R., Luo, K. (2015). An overview on fast pyrolysis of the main constituents in lignocellulosic biomass to valued-added chemicals: structures, pathways and interactions. *Renewable and Sustainable Energy Reviews, 51,* 761–774. DOI 10.1016/j.rser.2015.06.054.
8. Carrier, M., Windt, M., Ziegler, B., Appelt, J., Saake, B. et al. (2017). Quantitative insights into the fast pyrolysis of extracted cellulose, hemicelluloses, and lignin. *ChemSusChem, 10(16),* 3212–3224. DOI 10.1002/cssc.201700984.
9. Santos, F. M., Pires, J. C. M. (2018). Nutrient recovery from wastewaters by microalgae and its potential application as bio-char. *Bioresource Technology, 267,* 725–731. DOI 10.1016/j.biortech.2018.07.119.
10. Vélez, D. C. P., Magalhães, W. L. E., Capobianco, G. (2018). Carbon fiber from fast pyrolysis bio-oil. *Science and Technology of Materials, 30,* 16–22. DOI 10.1016/j.stmat.2018.10.001.
11. Cheng, S., Shu, J., Xia, H., Wang, S., Zhang, L. et al. (2019). Pyrolysis of crofton weed for the production of aldehyde rich bio-oil and combustible matter rich bio-gas. *Applied Thermal Engineering, 148,* 1164–1170. DOI 10.1016/j.applthermaleng.2018.12.009.
12. Dai, J., Cui, H., Grace, J. R. (2012). Biomass feeding for thermochemical reactors. *Progress in Energy and Combustion Science, 38(5),* 716–736. DOI 10.1016/j.pecs.2012.04.002.
13. Qureshi, K. M., Kay Lup, A. N., Khan, S., Abnisa, F., Wan Daud, W. M. A. (2018). A technical review on semi-continuous and continuous pyrolysis process of biomass to bio-oil. *Journal of Analytical and Applied Pyrolysis, 131,* 52–75. DOI 10.1016/j.jaap.2018.02.010.

14. Akhtar, J., Saidina Amin, N. (2012). A review on operating parameters for optimum liquid oil yield in biomass pyrolysis. *Renewable and Sustainable Energy Reviews, 16(7),* 5101–5109. DOI 10.1016/j.rser.2012.05.033.
15. Nzihou, A., Stanmore, B., Lyczko, N., Minh, D. P. (2019). The catalytic effect of inherent and adsorbed metals on the fast/flash pyrolysis of biomass: a review. *Energy, 170,* 326–337. DOI 10.1016/j.energy.2018.12.174.
16. Yang, H., Yao, J., Chen, G., Ma, W., Yan, B. et al. (2014). Overview of upgrading of pyrolysis oil of biomass. *Energy Procedia, 61,* 1306–1309. DOI 10.1016/j.egypro.2014.11.1087.
17. Papari, S., Hawboldt, K. (2018). A review on condensing system for biomass pyrolysis process. *Fuel Processing Technology, 180,* 1–13. DOI 10.1016/j.fuproc.2018.08.001.
18. Han, P., Jiang, E., Li, S. B., Wang, M. F., Sun, Y. et al. (2016). First-fractional bio-oil by fractional condensation of pyrolysis volatiles. *Transactions of the Chinese Society of Agricultural Machinery, 47,* 207–211.
19. Ma, S. W., Zhang, Y. M., Ding, H. Z., Zhu, X. F. (2018). Fractional condensation of biomass pyrolysis gas for multi-quality bio-oils. *Acta Energiae Solaris Sinica, 39,* 1367–1372.
20. Johansson, A. C., Iisa, K., Sandström, L., Ben, H., Pilath, H. et al. (2017). Fractional condensation of pyrolysis vapors produced from Nordic feedstocks in cyclone pyrolysis. *Journal of Analytical and Applied Pyrolysis, 123,* 244–254. DOI 10.1016/j.jaap.2016.11.020.
21. Huang, A. N., Hsu, C. P., Hou, B. R., Kuo, H. P. (2018). Production and separation of rice husk pyrolysis bio-oils from a fractional distillation column connected fluidized bed reactor. *Powder Technology, 323,* 588–593. DOI 10.1016/j.powtec.2016.03.052.
22. Li, J. (2010). The optimal of pyrolysis process in the rotating cone reactor and pyrolysis product analysis. *International Conferences of Challenges Environment and Science Computer Engineering, 1,* 530–533.
23. Pollard, A. S., Rover, M. R., Brown, R. C. (2012). Characterization of bio-oil recovered as stage fractions with unique chemical and physical properties. *Journal of Analytical and Applied Pyrolysis, 93,* 129–138. DOI 10.1016/j.jaap.2011.10.007.
24. Tumbalam Gooty, A., Li, D., Briens, C., Berruti, F. (2014). Fractional condensation of bio-oil vapors produced from birch bark pyrolysis. *Separation and Purification Technology, 124,* 81–88. DOI 10.1016/j.seppur.2014.01.003.
25. Kim, P., Weaver, S., Labbé, N. (2016). Effect of sweeping gas flow rates on temperature-controlled multistage condensation of pyrolysis vapors in an auger intermediate pyrolysis system. *Journal of Analytical and Applied Pyrolysis, 118,* 325–334. DOI 10.1016/j.jaap.2016.02.017.
26. Yin, R., Liu, R., Mei, Y., Fei, W., Sun, X. (2013). Characterization of bio-oil and bio-char obtained from sweet sorghum bagasse fast pyrolysis with fractional condensers. *Fuel, 112,* 96–104. DOI 10.1016/j.fuel.2013.04.090.
27. Chen, T., Deng, C., Liu, R. (2010). Effect of selective condensation on the characterization of bio-oil from pine sawdust fast pyrolysis using a fluidized-bed reactor. *Energy & Fuels, 24(12),* 6616–6623. DOI 10.1021/ef1011963.
28. Guo, Z., Wang, S., Gu, Y., Xu, G., Li, X. et al. (2010). Separation characteristics of biomass pyrolysis oil in molecular distillation. *Separation and Purification Technology, 76(1),* 52–57. DOI 10.1016/j.seppur.2010.09.019.
29. Wang, S., Gu, Y., Liu, Q., Yao, Y., Guo, Z. et al. (2009). Separation of bio-oil by molecular distillation. *Fuel Processing Technology, 90(5),* 738–745. DOI 10.1016/j.fuproc.2009.02.005.
30. Choi, J. H., Kim, S.-S., Woo, H. C. (2017). Characteristics of vacuum fractional distillation from pyrolytic macroalgae (*Saccharina japonica*) bio-oil. *Journal of Industrial and Engineering Chemistry, 51,* 206–215. DOI 10.1016/j.jiec.2017.03.002.
31. Jendoubi, N., Broust, F., Commandre, J. M., Mauviel, G., Sardin, M. et al. (2011). Inorganics distribution in bio oils and char produced by biomass fast pyrolysis: the key role of aerosols. *Journal of Analytical and Applied Pyrolysis, 92(1),* 59–67. DOI 10.1016/j.jaap.2011.04.007.
32. Iisa, K., Johansson, A.-C., French, E. P. R. J., Ortona, K. A., Wiinikka, H. (2019). Chemical and physical characterization of aerosols from fast pyrolysis of biomass. *Journal of Analytical and Applied Pyrolysis, 142,* 104606. DOI 10.1016/j.jaap.2019.04.022.

33. Ordou, N., Agranovski, I. E. (2017). Mass distribution and elemental analysis of the resultant atmospheric aerosol particles generated in controlled biomass burning processes. *Atmospheric Research, 198,* 108–112. DOI 10.1016/j.atmosres.2017.08.015.
34. Dauenhauer, P., Teixeira, A., Gantt, R., Joseph, K., Maduskar, S. et al. (2016). Spontaneous aerosol ejection: origin of inorganic particles in biomass pyrolysis. *ChemSusChem, 9(11),* 1322–1328. DOI 10.1002/cssc.201600112.
35. Wiinikka, H., Johansson, A-C., Sandström, L., Öhrman, O. G. W. (2017). Fate of inorganic elements during fast pyrolysis of biomass in a cyclone reactor. *Fuel, 203,* 537–547. DOI 10.1016/j.fuel.2017.04.129.
36. Laskin, A., Laskin, J., Nizkorodov, S. (2015). Chemistry of atmospheric brown carbon. *Chemical Reviews, 115(10),* 4335–4382. DOI 10.1021/cr5006167.
37. Li, X., Chen, Y., Bond, T. C. (2016). Light absorption of organic aerosol from pyrolysis of corn stalk. *Atmospheric Environment, 144,* 249–256. DOI 10.1016/j.atmosenv.2016.09.006.
38. Chen, Y., Bond, T. C. (2010). Light absorption by organic carbon from wood combustion. *Atmospheric Chemistry and Physics, 10(4),* 1773–1787. DOI 10.5194/acp-10-1773-2010.
39. Gong, X., Zhang, C., Chen, H., Nizkorodov, S., Chen, J. et al. (2015). Size distribution and mixing state of black carbon particles during a heavy air pollution episode in Shanghai. *Atmospheric Chemistry & Physics, 15,* 35383–35415.
40. Lack, D. M., Langridge, J. (2013). On the attribution of black and brown carbon light absorption using the Ångström exponent. *Atmospheric Chemistry and Physics, 13(6),* 15493–15515.
41. Rajesh, T. A., Ramachandran, S. (2018). Black carbon aerosols over urban and high altitude remote regions: characteristics and radiative implications. *Atmospheric Environment, 194,* 110–122. DOI 10.1016/j.atmosenv.2018.09.023.
42. Xie, M., Shen, G., Holder, A. L., Hays, M. D., Jetter, J. J. (2018). Light absorption of organic carbon emitted from burning wood, charcoal, and kerosene in household cookstoves. *Environmental Pollution, 240,* 60–67. DOI 10.1016/j.envpol.2018.04.085.
43. Yao, Z., You, S., Dai, Y., Wang, C. H. (2018). Particulate emission from the gasification and pyrolysis of biomass: concentration, size distributions, respiratory deposition-based control measure evaluation. *Environmental Pollution, 242,* 1108–1118. DOI 10.1016/j.envpol.2018.07.126.
44. Li, Z., Li, N., Yi, W., Fu, P., Li, Y. et al. (2016). Design and operation of a down-tube reactor demonstration plant for biomass fast pyrolysis. *Fuel Processing Technology, 161,* 182–192. DOI 10.1016/j.fuproc.2016.12.014.
45. Fu, F., Shinohaya, N., Ito, M., Xu, X., Shen, M. et al. (2008). Difference between low-volume and high-volume Andersen samplers in measuring atmospheric aerosols. *Particuology, 6(3),* 218–222. DOI 10.1016/j.partic.2008.01.005.
46. Zhai, M., Wang, X., Zhang, Y., Dong, P., Qi, G. (2015). Characteristics of rice husk tar pyrolysis by external flue gas. *International Journal of Hydrogen Energy, 40(34),* 10780–10787. DOI 10.1016/j.ijhydene.2015.07.045.
47. Heo, H. S., Park, H. J., Park, Y.-K., Ryu, C., Suh, D. J. et al. (2010). Bio-oil production from fast pyrolysis of waste furniture sawdust in a fluidized bed. *Bioresource Technology, 101(1),* S91–S96. DOI 10.1016/j.biortech.2009.06.003.
48. Cai, W., Dai, L., Liu, R. (2018). Catalytic fast pyrolysis of rice husk for bio-oil production. *Energy, 154,* 477–487. DOI 10.1016/j.energy.2018.04.157.
49. Collard, F.-X., Blin, J. (2014). A review on pyrolysis of biomass constituents: mechanisms and composition of the products obtained from the conversion of cellulose, hemicelluloses and lignin. *Renewable and Sustainable Energy Reviews, 38,* 594–608. DOI 10.1016/j.rser.2014.06.013.
50. Zhang, H., Gao, Z., Ao, W., Li, J., Liu, G. et al. (2017). Microwave pyrolysis of textile dyeing sludge in a continuously operated auger reactor: char characterization and analysis. *Journal of Hazardous Materials, 334,* 112–120. DOI 10.1016/j.jhazmat.2017.03.048.
51. Wang, S., Dai, G., Yang, H., Luo, Z. (2017). Lignocellulosic biomass pyrolysis mechanism: a state-of-the-art review. *Progress in Energy and Combustion Science, 62,* 33–86. DOI 10.1016/j.pecs.2017.05.004.

52. Lv, G., Wu, S., Yang, G., Chen, J., Liu, Y. et al. (2013). Comparative study of pyrolysis behaviors of corn stalk and its three components. *Journal of Analytical and Applied Pyrolysis, 104,* 185–193. DOI 10.1016/j.jaap.2013.08.005.
53. Grewal, A., Abbey, L., Gunupuru, L. R. (2018). Production, prospects and potential application of pyroligneous acid in agriculture. *Journal of Analytical and Applied Pyrolysis, 135,* 152–159. DOI 10.1016/j.jaap.2018.09.008.
54. Johnson, D. R. (2016). Nanometer-sized emissions from municipal waste incinerators: a qualitative risk assessment. *Journal of Hazardous Materials, 320,* 67–79. DOI 10.1016/j.jhazmat.2016.08.016.
55. Huang, Y., Wei, Z., Qiu, Z., Yin, X., Wu, C. (2012). Study on structure and pyrolysis behavior of lignin derived from corncob acid hydrolysis residue. *Journal of Analytical and Applied Pyrolysis, 93,* 153–159. DOI 10.1016/j.jaap.2011.10.011.
56. Faravelli, T., Frassoldati, A., Migliavacca, G., Ranzi, E. (2010). Detailed kinetic modeling of the thermal degradation of lignins. *Biomass and Bioenergy, 34(3),* 290–301. DOI 10.1016/j.biombioe.2009.10.018.
57. Kirchstetter, T., Novakov, T. V., Hobbs, P. (2004). Evidence that the spectral dependence of light absorption by aerosols is affected by organic carbon. *Journal of Geophysical Research: Atmospheres, 109(D21),* 21208. DOI 10.1029/2004JD004999.
58. Chakrabarty, R. K., Moosmüller, H., Chen, L. W. A., Lewis, K., Arnott, W. P. et al. (2010). Brown carbon in tar balls from smoldering biomass combustion. *Atmospheric Chemistry and Physics, 10(13),* 6363–6370. DOI 10.5194/acp-10-6363-2010.